NSRRC - J04880 (>015)

Thin Solid Films 590 (2015) 1–6

Contents lists available at ScienceDirect

Thin Solid Films

journal homepage: www.elsevier.com/locate/tsf

Pore morphology of low-k SiC_xN_y films prepared with a cyclic silazane precursor using plasma-enhanced chemical vapor deposition

Hung-En Tu [a], Chun-Jen Su [b], U-Ser Jeng [b], Jihperng Leu [a,*]

[a] Department of Materials Science and Engineering, National Chiao Tung University, 1001 University Road, Hsinchu 30010, Taiwan
[b] National Synchrotron Radiation Research Center, 101 Hsin-Ann Road, Hsinchu Science Park, Hsinchu 30076, Taiwan

ARTICLE INFO

Article history:
Received 5 August 2014
Received in revised form 27 January 2015
Accepted 17 July 2015
Available online 21 July 2015

Keywords:
Low-k
Silicon carbonitride
Thin Films
Pore morphology
Grazing-incidence small-angle X-ray scattering

ABSTRACT

Low-k SiC_xN_y films were prepared using radio-frequency plasma-enhanced chemical vapor deposition (PECVD), with only 1,3,5-trimethyl-1,3,5-trivinylcyclotrisilazane (VSZ) as the precursor; VSZ has cyclic Si–N–Si linkages and three pendent vinyl groups. At lower PECVD temperatures, SiC_xN_y films possess relatively low film densities, indicating the existence of a loose structure or voids within the cross-linked matrix structure. The pore morphology of SiC_xN_y films deposited at distinct temperatures were examined using grazing-incidence small-angle X-ray scattering, while the chemical bondings and structural information were analyzed using Fourier-transform infrared spectroscopy. At 100 °C, SiC_xN_y films without porogen displaying 4.9 nm pores and a mean pore spacing of 30.1 nm generated low-density films because Si-$(CH_2)_n$-Si and/or Si-$(CH_2)_n$-CH_3 could be incorporated free volume into the N–Si–C cross-linked structure under plasma deposition. At 300 °C, the N–Si–C cross-linked structure and the some organic phase were disrupted and transformed into a denser structure, reducing pore size (3.5 nm) and losing pore correlation. Thus, low deposition temperatures facilitate the formation of large pores and the ordering of the pores. Post annealing converted the 100 and 300 °C as-deposited SiC_xN_y films into loose and dense structures, respectively, and maintained slightly reduced pore size and pore correlation in the annealed films.

© 2015 Elsevier B.V. All rights reserved.

1. Introduction

As integrated-circuit dimensions are continually scaled down, the increase in propagation (RC) delay, crosstalk noise, and power dissipation in the interconnection become the limiting factors in the design of ultra-large-scale integrated devices [1]. To reduce the effective capacitance (k_{eff}) in the copper backend interconnection, low-k etch-stop/dielectric barrier materials such as silicon carbonitride (SiC_xN_y) ($k = 4.5–5.5$) [2] have been introduced in 45 nm nodes and beyond, following the implementation of low-k inter-layer dielectric (ILD) materials such as carbon-doped oxide and ultra-low-k dielectrics [3] and the scaling of their thickness [4,5]. Silicon carbonitride films have been typically prepared using plasma-enhanced chemical vapor deposition (PECVD) of multi-precursors such as $SiH_4 + NH_3$ (or N_2) + CH_4 [6,7] and $SiH(CH_3)_3 + NH_3$ [8]. Recently, single source precursors such as hexamethyldisilazane (HMDS) [9,10], and BASICN™ [11] have been examined for use in low-k SiC_xN_y applications, because compared with multi-precursors, single source precursors retain higher C content to achieve lower polarizability and improved etch selectivity. However, their dielectric constant values (4.5 to 3.8) are still too high for future integrations even their thickness is scaled down. To further reduce the dielectric constant of silicon carbonitride materials, the primary approach is to reduce the film density, in addition to the continued increase of C/Si ratio. A similar approach has been demonstrated for low-k SiC_xO_y inter-layer dielectric films by using single precursors with volumic cyclic structures, such as a 6, 8, or 10-membered Si–O ring [12,13] to introduce intrinsic and induced porosity for lowering the film's density.

This prompts us to explore a cyclic N–Si–N silazane precursor for a lower k SiC_xN_y films. In specific, 1,3,5-trimethyl-1,3,5-trivinylcyclotrisilazane (VSZ) with 3 vinyl side-groups was used as a single precursor using radio-frequency (RF) PECVD technique at a low power density (0.15 W/cm^3). The deposition temperatures ranging from 25 to 400 °C yield low-k SiC_xN_y films with k from 3.6 to 4.6 [14]. Their film densities were 1.6–2.0 g/cm^3, which are considerably lower than the density of Si_3N_4 films ($k = 7.5$; $\rho = 3.1$ g/cm^3) [15] or SiC_xN_y (BASICN™ 400) films ($k = 4.3$; $\rho = 1.86$ g/cm^3) [11]. The low density of these SiC_xN_y films using VSZ precursor at low deposition temperatures indicates the existence of a loose structure or voids within the cross-linked matrix structure. Such SiC_xN_y films are of great interest as etch-stop/diffusion barrier in the copper interconnects because there is no need of adding a sacrificial porogen and post-treatment for removing the porogen. Yet, the origin of the low density of these SiC_xN_y films and the information about pore size and pore size distribution are still vague.

Although ellipsometric porosimetry [16] and positron annihilation spectroscop [17] have been successfully used in pore size characterization, a non-destructive, grazing-incidence small-angle X-ray scattering (GISAXS) technique can offer complete information of the pore shape,

* Corresponding author.
E-mail address: jimleu@mail.nctu.edu.tw (J. Leu).

http://dx.doi.org/10.1016/j.tsf.2015.07.036
0040-6090/© 2015 Elsevier B.V. All rights reserved.

pore sizes, and pore size distribution, and any periodic pattern [18,19]. Thus, in this study, the pore morphology was examined using GISAXS and the chemical structures of the 100 and 300 °C as-deposited SiC_xN_y films were examined using Fourier-transform infrared (FTIR) spectroscopy. Moreover, the change in pore morphology induced by annealing performed at 400 °C for 3 h was investigated and discussed.

2. Experimental

PECVD was used to deposit SiC_xN_y films onto a silicon wafer by using a liquid monomer, VSZ (Gelest, Inc. 95%), as the matrix precursor. The deposition was performed in an RF (13.56 MHz) parallel-plate PECVD system. VSZ was vaporized at 60 °C to prevent condensation in the pipe and was then carried into the reactor by an Ar carrier gas. The deposition pressure and RF power were maintained at 12 Pa (90 mTorr) and 50 W (power density = 0.15 W/cm^3), respectively, without bias. The deposition temperatures were varied from 100 to 300 °C. Subsequently, the annealing step was performed at 400 °C for 3 h under an Ar atmosphere to generate the as-deposited SiC_xN_y films.

The chemical bondings of the SiC_xN_y films were examined using FTIR spectroscopy (MAGNA-IR Technology Protege 460) at a normal incident angle under the transmission mode. The FTIR spectra were collected using a total of 32 scans in the 500–4000 cm^{-1} range, at a resolution of 4 cm^{-1}.

Pore morphology was characterized using the GISAXS system at the BL23A beam-line of the National Synchrotron Radiation Research Center, Taiwan. All 2D GISAXS patterns were recorded using a Pilatus 1 M-F area detector, with an incident angle of 0.2° of the 10 keV X-ray beam (0.5 mm diameter); SAXS data were analyzed using the Guinier approximation to determine the size of the pores [20].

The densities of the porous SiC_xN_y films were calculated using an X-ray reflectivity (XRR) instrument (Bruker D8 Discover) equipped with a Cu K_α source ($\lambda = 0.154$ nm). The scanning region ranged from 0° to 2°. The XRR data were analyzed using LEPTOS simulation software to fit the density of the SiC_xN_y film.

3. Results and discussion

In order to understand the growth mechanism of the SiC_xN_y films prepared by PECVD using VSZ precursor, the deposition rate of SiC_xN_y films as a function of deposition temperatures was first examined and illustrated in Fig. 1. The deposition rate of SiC_xN_y films increased with increasing deposition temperature up to 200 °C, after which the deposition rate slightly decreased. It exhibited two types of growth mechanism; namely, surface-reaction-controlled growth between 25 and 200 °C, while mass-transfer-controlled growth between 200 and 400 °C.

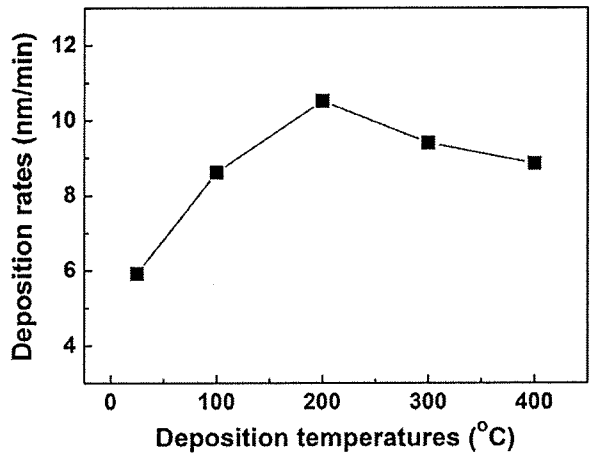

Fig. 1. Deposition rate of the SiC_xN_y films as a function of deposition temperatures.

GISAXS was used to examine the pore morphology of low-k SiC_xN_y films as-deposited at 100 and 300 °C and to study any additional change in morphology after annealing the films at 400 °C for 3 h. Fig. 2 presents the 2D GISAXS patterns of the low-k SiC_xN_y films as-deposited at 100 and 300 °C and after annealing at 400 °C for 3 h. The scattering images of the SiC_xN_y films as-deposited at 100 °C and after annealing at 400 °C (Fig. 2a and b) display two notable vertical streaks in the lateral direction, revealing a highly ordered structure possessing a mean spacing, as detailed in the following paragraph. By contrast, no ordered peaks were observed when examining films deposited at 300 °C and then annealed at 400 °C (Fig. 2c and d). The vertical streak in the GISAXS pattern indicates a spatially ordered arrangement in which the distance between pores is correlated in the horizontal direction [21, 22], but not in the vertical direction, in films deposited at a low temperature (100 °C); this spatial ordering was absent in films deposited at higher temperatures such as 300 °C. Moreover, no noticeable change was detected in the scattering patterns of as-deposited films (Fig. 2a and c) and post-annealed films (Fig. 2b and d).

Next, the in-plane and out-of-plane intensities of the scattering patterns (Fig. 2) were extracted, and their corresponding GISAXS scattering profiles relative to scattering wavevector (q) are presented in Figs. 3 and 4. At the low-q regions of the in-plane scattering profiles of SiC_xN_y films deposited at 100 °C (Fig. 3a), the intensity peak revealed a spatial arrangement of pores displaying a specific correlation distance. The maximal intensities of SiC_xN_y films as-deposited at 100 °C and post-annealed appeared at q_p values of 0.2085 and 0.2128 nm^{-1}, respectively. Using the formula $L = 2\pi/q_p$ [22], the dominant mean distances between pores were estimated to be 30.1 and 29.5 nm for as-deposited and post-annealed films, respectively, which resulted from the occurrence of a marginally short-range ordering, parallel to the sample surface. The result also shows that an ordered and rigid pore structure of the film can be maintained at the high post-annealing temperature of 400 °C for 3 h.

In the case of the SiC_xN_y films deposited at 300 °C and post-annealed at 400 °C, no maximal intensity peak was detected in the profiles (Fig. 4a), suggesting that the pores in these films were randomly distributed.

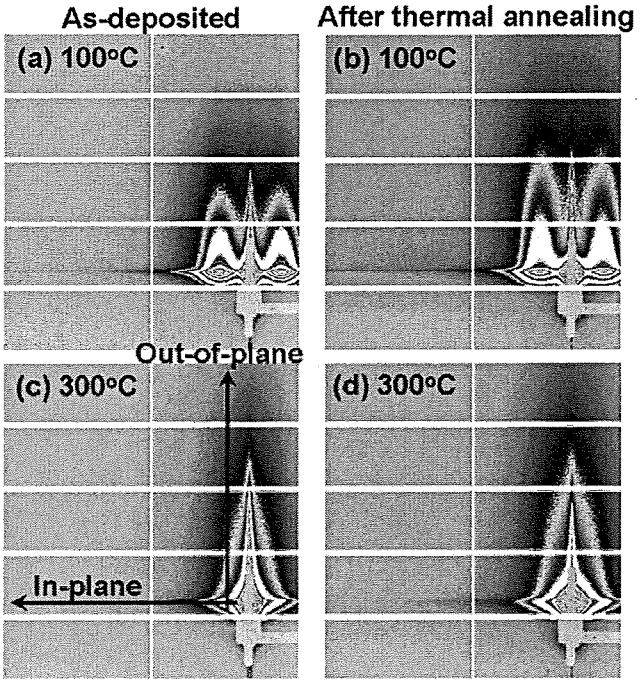

Fig. 2. 2D GISAXS scattering patterns of the SiC_xN_y films at different deposition temperatures: 100 °C and 300 °C, using only VSZ precursor, as-deposited and after thermal annealing at 400 °C.

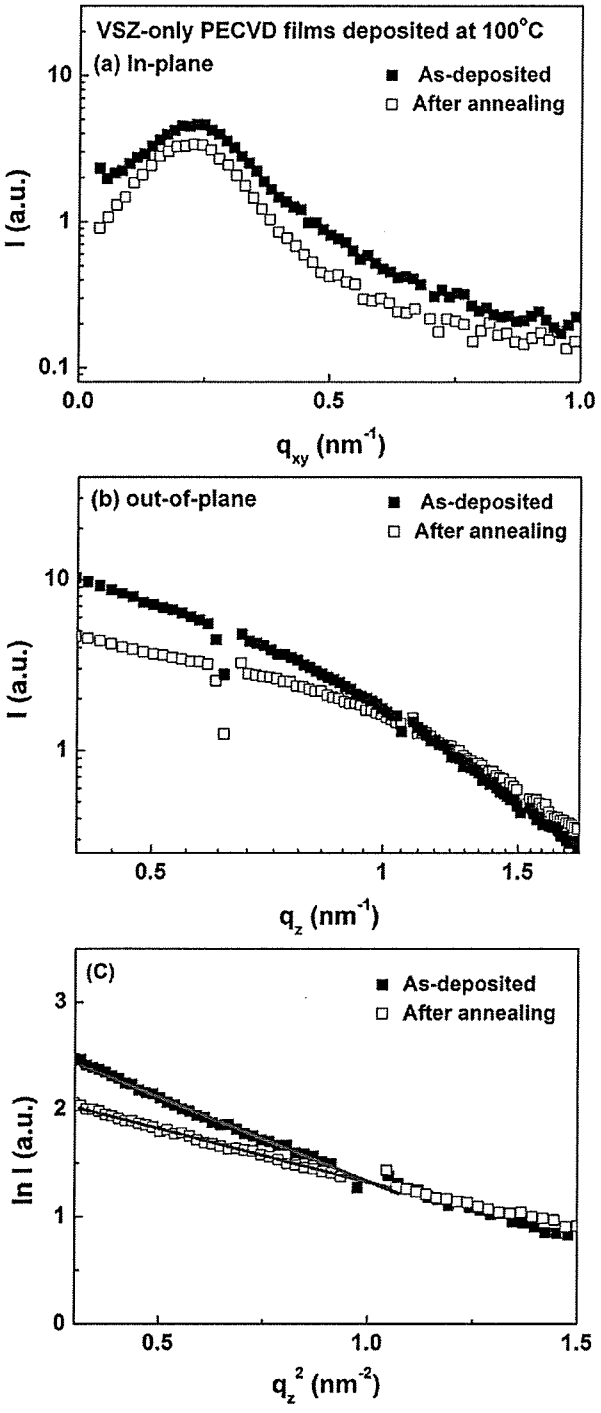

Fig. 3. GISAXS scattering profiles of the SiC_xN_y films at 100 °C, using only VSZ precursor, as-deposited and after thermal annealing at 400 °C: (a) in-plane, (b) out-of-plane scattering direction, and (c) Guinier plots (ln I vs. q_z^2) from the out-of-plane scattering profiles. The solid lines were obtained by fitting the data using the Guinier approximation.

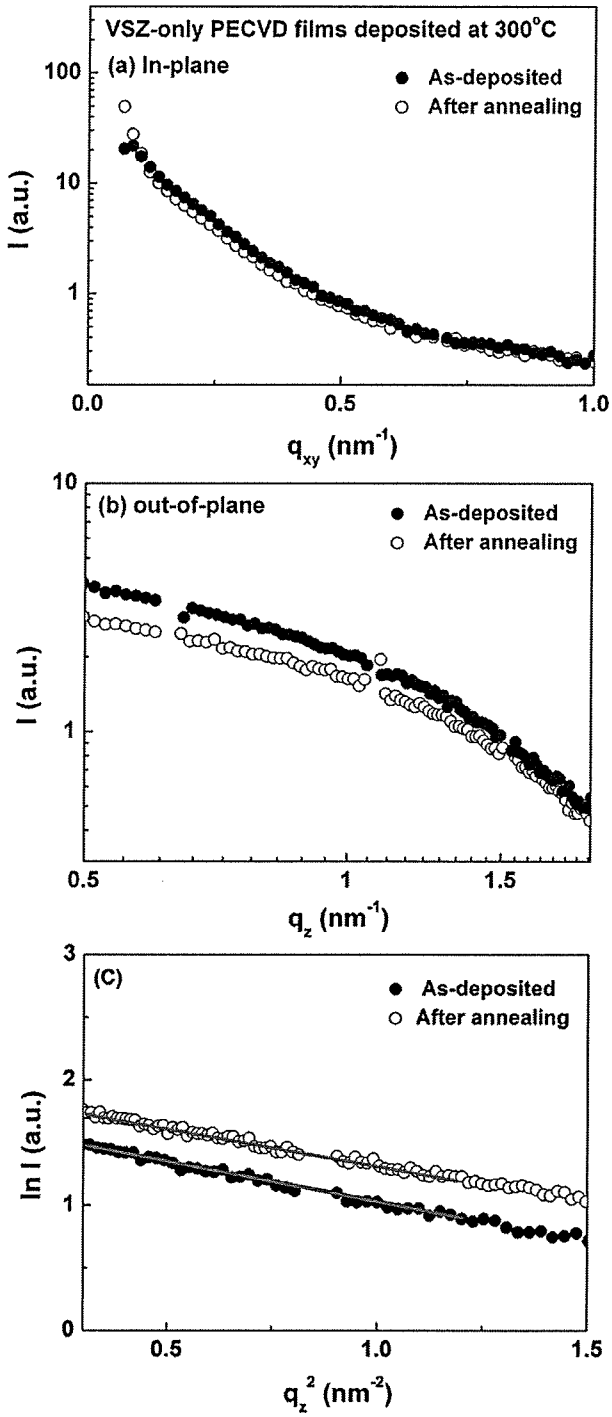

Fig. 4. GISAXS scattering profiles of the SiC_xN_y films at 300 °C, using only VSZ precursor, as-deposited and after thermal annealing at 400 °C: (a) in-plane, (b) out-of-plane scattering direction, and (c) Guinier plots (ln I vs. q_z^2) from the out-of-plane scattering profiles. The solid lines were obtained by fitting the data using the Guinier approximation.

Furthermore, the out-of-plane scattering profiles of the films differed only slightly (Fig. 4b), which is addressed in the following section.

The scattering patterns were further analyzed using a particulate system to quantify pore geometries [23]. The scattering intensity of an individual particle, $I(q)$, is described by Eq. (1):

$$I(q) = n_p\left(\rho_p - \rho_m\right)^2 V_p^2 P(q) S(q) \tag{1}$$

where the scattering wavevector $q = 4\pi\lambda^{-1}\sin\theta$ is defined by the wavelength (λ) and the scattering angle (θ) of the X-ray; n_p is the number density of the particles; ρ_p and ρ_m are the scattering densities of the particle and the matrix, respectively; V_p denotes particle volume (pore volume in this case); and $P(q)$ is a form factor and $S(q)$ is a structure factor. When the particle or pore concentration is low, the particles/pores scattered in the film do not interact with each other, and thus the structure factor $S(q)$ is close to 1 and can be ignored. Therefore, the scattering

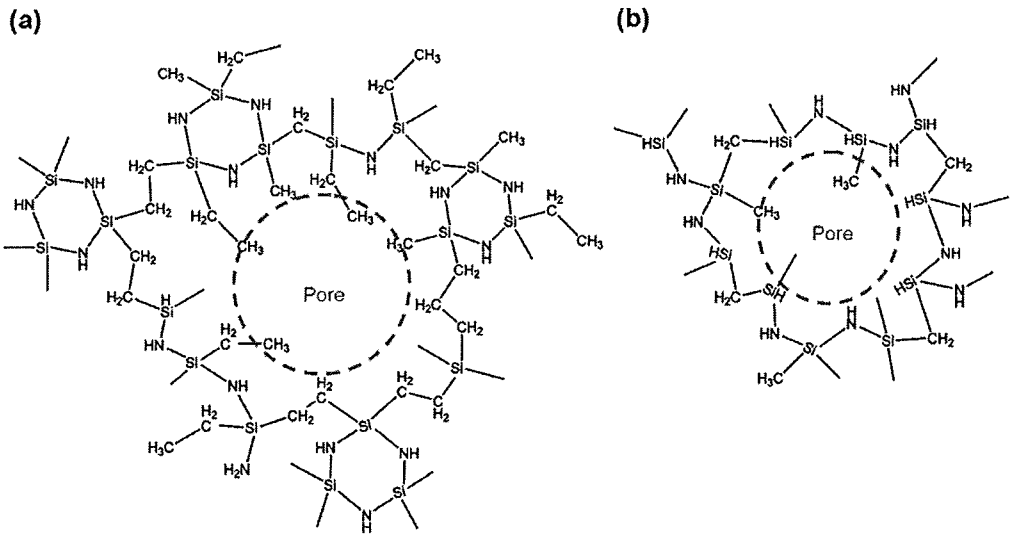

Fig. 5. Schematic representation of different pore structures in SiC_xN_y films as-deposited at (a) 100 °C, and (b) 300 °C.

intensity $I(q)$ is only dominated by the form factor $P(q)$ of the particles/pores. For approximation, $I(q)$ can be reduced to the Guinier expression [24,25] used for a radius of gyration R_g, as described by Eq. (2):

$$I(q) = n_p\left(\rho_p - \rho_m\right)^2 V_p^2 \exp\left(\frac{-q^2R_g^2}{3}\right). \quad (2)$$

The scattering profile in the horizontal direction could not be used to extract well-defined pore geometries by using Guinier approximation because both the form factor $P(q)$ and the structure factor $S(q)$ contributed in the same q region. Hence, the pore sizes were obtained from the scattering profiles in the out-of-plane direction (Figs. 3b and 4b), without the interference of the structure factor. The Guinier approximation fit the scattering profiles well (Figs. 3c and 4c), which indicates that only a mono-dispersed pore size was present in the low-k SiC_xN_y films prepared using VSZ, even when no porogen was added. In this case, R_g values were extracted from the linear relationship between ln (I) and q_z^2 in the Guinier approximation. Assuming spherical pores, the pore size was further deduced as $D = 2(5/3)^{0.5}R_g$. Thus, the pore sizes (D) in SiC_xN_y films as-deposited at 100 and 300 °C were determined to be 4.9 ± 0.4 and 3.5 ± 0.3 nm, respectively. After thermal annealing, the pores in the SiC_xN_y films deposited at 100 and 300 °C shrank slightly to 4.1 ± 0.4 and 3.3 ± 0.2 nm, respectively.

Since there is little work on porous SiC_xN_y films, the pore sizes of as-deposited SiC_xN_y films in this study were compared to PECVD porous SiCOH films prepared using single precursor [12,13] and/or conventional approach using a precursor and an oxidant [26] The pore sizes in our study were found to be larger than SiCOH films prepared using single precursor [12,13]. Tada et al. [12] reported PECVD porous SiOCH films with pore sizes ranging from 0.39 to 0.66 nm using a ring-type siloxane precursor with both of the vinyl and the alkyl side-groups at 350 °C and under high pressure and low-power plasma condition to preserve the original ring-type chemical structure. C. H. Lo et al. [13] reported SiCOH film prepared by using octamethylcyclotetrasiloxane (OMCTS) and pore diameter 0.74–0.76 nm for the matrix structure and 0.6–0.7 nm for big cages. The formation of big cages was attributed to the linear chains and short fragments from the breakup of the cyclic rings [13]. To elucidate the formation mechanism of the relatively large pores in our study, we refer to FTIR analysis of such SiC_xN_y films as-deposited at 100 °C and 300 °C in our previous work [14]. At low deposition temperatures (≤200 °C), most of the cyclic structures of VSZ were preserved in the SiC_xN_y films after the PECVD process. Still, some of the cyclic N—Si—N bonds were opened and broken into the small fragments such as –Si–N– [14]. Moreover, during the plasma deposition process, the vinyl side-groups in VSZ could be readily activated and reacted to form the long organic chain, such as Si-$(CH_2)_n$-Si and/or Si-$(CH_2)_n$-CH_3 [14,26,27]. Meanwhile, it probably also reacted with the fragment of –Si–N– to form the N–Si–C cross-linked structures. Thus, the N–Si–C cross-linked structures function as the matrix, while long organic chain could be incorporated as free volume, i.e. induced pores (4.9 ± 0.4 nm) in the SiC_xN_y films, as schematically illustrated by Fig. 5(a). The large pores (4.9 ± 0.4 nm) along with a pore correlation distance, 30.1 nm, can account for the low density of the SiC_xN_y film (1.67 g/cm^3). In contrast, for the 300 °C as-deposited SiC_xN_y film, most of the organic chain and N–Si–C linkage structures were eliminated, according to the infrared analysis in our previous work [14]. In addition, the cyclic N–Si–N linkages of VSZ were completely transformed into a dense Si–N structure. Because of the disappearance of some of the long organic chains upon deposition and N–Si–C linkage structures into more dense Si–N structure, the pores were smaller (3.5 ± 0.3 nm) and randomly distributed in the films deposited at 300 °C, as schematically illustrated in Fig. 5(b).

We then carried out FT-IR analysis of SiC_xN_y films post-annealed at 400 °C for 3 h to understand the post-annealing effect on the pore size

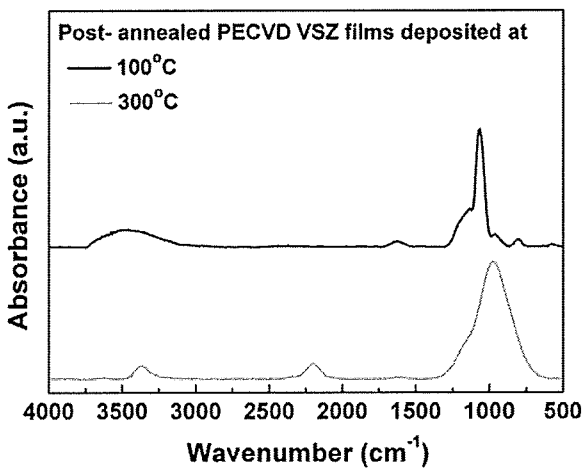

Fig. 6. FTIR spectra of VSZ-only PECVD films prepared at 100 °C and 300 °C with post annealing at 400 °C for 3 h.

Table 1
GISAXS detailed analyses and properties of low-k SiC_xN_y films.

Deposition temperature	As-deposited			After thermal annealing at 400 °C, 3 h		
	D (nm)	*L* (nm)	Film density	*D* (nm)	*L* (nm)	Film density
100 °C	4.9 ± 0.4	30.1	1.67	4.1 ± 0.4	29.5	1.63
300 °C	3.5 ± 0.3	–	1.83	3.3 ± 0.2	–	1.87

of SiC_xN_y films. The FTIR spectrum of post-annealed SiC_xN_y film (upper spectrum in Fig. 6) showed that the symmetric stretching vibration of the C—H_2 bond at 2879 cm^{-1} [28,29], the asymmetric stretching vibration of the C—H_2 bond at 2933 cm^{-1} [29], the asymmetric stretching vibration of the C—H_3 bond at 2962 cm^{-1} [28], and the bending vibration of Si—CH_3 bonds at 1265 cm^{-1} [10,30] nearly disappeared. Furthermore, the intensities of the N-H bands at 3370 and 1150 cm^{-1} (1625 cm^{-1} CN-H) [31,32] decreased. These changes indicated that labile pendent groups, such as the CH_x group (x = 2 or 3), bonded to Si and the N—H bonds became volatile during the annealing process and generated intrinsic volume. By contrast, the main Si–N–Si peak was shifted from 1047 to 1067 cm^{-1} after annealing. The blue shift was likely caused by an increase in the Si—N—Si bond angle as a result of two possible mechanisms: 1) the film structures were loosened because of the desorption of CH_4, H_2, and possibly NH_3 as a result of the chain scissions occurring at the Si-CH_x and N—H bonds [14,29] under annealing; and 2) the C—Si bonds, adjacent to the Si—N—Si bonds, were broken and then bonded to N atoms, which have larger electronegativity than C atoms do [29]. Consequently, the organic phases were eliminated as intrinsic volume, whereas the matrix of the Si–N cross-linked structure was increasingly formed after the annealing step. After thermal annealing, the pores became smaller (4.1 ± 0.4 nm, compared with 4.9 ± 0.4 nm before annealing) and the pore correlation distance decreased (to 29.5 nm, from 30.1 nm before annealing), which are summarized in Table 1.

When the films as-deposited at 300 °C were annealed at 400 °C for 3 h (upper spectrum in Fig. 6), the organic CH_x phases and N—H bonds in the films were burnt out. However, the disparity in bonding before and after annealing was considerably smaller because the structures deposited at the high deposition temperature were more stable and dense than those deposited at lower deposition temperature. Conversely, the main Si–N–Si absorption was red-shifted from 1043 to 1019 cm^{-1}, shown in Fig. 6. This can be attributed to the films becoming denser after annealing, at which point the film density was 1.87 g/cm^3 compared with 1.83 g/cm^3 for the film as-deposited at 300 °C, which are summarized in Table 1. Moreover, the pore size decreased only slightly, from 3.5 ± 0.3 nm before to 3.3 ± 0.2 nm after annealing.

In summary, low-k SiC_xN_y films prepared by using PECVD of VSZ precursor, without the use of porogen, could fabricate the mesoporous structures with pore sizes in the range of 3.3–4.9 nm. Diverse pore morphologies could be obtained by tuning the deposition temperature, as summarized in Table 1. The formation mechanism of the pore structures were mainly dominated by the formation of long organic chain, such as Si-$(CH_2)_n$-Si and/or Si-$(CH_2)_n$-CH_3, through the readily activated vinyl side-groups and the fragments of broken cyclic bonds, instead of intrinsic molecular-structures porosity. The mesoporous SiC_xN_y films fabricated in this work are suitable candidate for use as the low-k etch-stop layer to further reduce the k_{eff} in the copper dual damascene backend interconnects.

4. Conclusion

Low-k porous SiC_xN_y films were prepared by performing PECVD at 100 and 300 °C and using only 1,3,5-trimethyl-1,3,5-trivinylcyclotrisilazane as the precursor, which possesses a cyclic Si–N–Si linkage, a pendent CH_x phase and three vinyl side-groups. At low deposition temperatures (≤200 °C), most of the cyclic structures of VSZ were preserved in the SiC_xN_y films after the PECVD process. Still, some of the cyclic N—Si—N bonds were opened and broken into the small fragments such as –Si–N–. During the plasma deposition process, the vinyl side-groups in VSZ could be readily activated and reacted to form the long organic chain, such as Si-$(CH_2)_n$-Si and/or Si-$(CH_2)_n$-CH_3, meanwhile it probably reacted with the fragment of –Si–N– and formed the N–Si–C cross-linked structures. At a deposition temperature of 100 °C, an average pore size of 4.9 ± 0.4 nm and a short-range ordering of the pores (mean pore spacing, 30.1 nm) in a direction parallel to the film surface were exhibited. At high deposition temperature of 300 °C, most of the organic chain and N–Si–C cross-linked structures were elimination, which resulted in the formation of films with smaller pores (3.5 ± 0.3 nm) that did not display short-range ordering (i.e., the pores are randomly distributed). In addition, ordered and rigid pore structures of SiC_xN_y films can be maintained after the high post-annealing treatment.

Acknowledgments

The authors are grateful for the financial support provided by the Ministry of Science and Technology, ROC, under Contract No. NSC 101-2221-E-009-126-MY2 and MOST 103-2221-E-009-181-MY3. The technical discussion with Dr. Wen-Li Wu of the National Institute of Standards and Technology (NIST), USA is also appreciated.

References

[1] M.T. Bohr, Interconnect scaling – the real limiter to high performance ULSI, Solid State Technol. 39 (1996) 105–111.
[2] C.C. Chiang, M.C. Chen, Z.C. Wu, L.J. Li, S.M. Jang, C.H. Yu, M.S. Liang, TDDB reliability improvement of Cu damascene with a bilayer structured a SiC:H dielectric barrier, J. Electrochem. Soc. 151 (2) (2004) G89–G92.
[3] P. Moon, V. Chikarmane, K. Fischer, R. Grover, T.A. Ibrahim, D. Ingerly, K.J. Lee, C. Litteken, T. Mule, S. Williams, Process and electrical results for the on-die interconnect stack for Intel's 45 nm process generation, Intel Technol. J. 12 (2008) 87–92.
[4] D. Ingerly, A. Agrawal, R. Ascazubi, A. Blattner, M. Buehler, V. Chikarmane, B. Choudhury, F. Cinnor, C. Ege, C. Ganpule, T. Glassman, R. Grover, P. Hentges, J. Hicks, D. Jones, A. Kandas, H. Khan, N. Lazo, K.S. Lee, H. Liu, A. Madhavan, R. McFadden, T. Mule', D. Parsons, P. Parthangal, S. Rangaraj, D. Rao, J. Roesler, A. Schmitz, M. Sharma, J. Shin, Y. Shusterman, N. Speer, P. Tiwari, G. Wang, P. Yashar, K. Mistry, Low-k interconnect stack with metal-insulator-metal capacitors for 22 nm high volume manufacturing, Conference Proceedings of the IEEE International Interconnect Technology (IITC), 2012.
[5] R. Brain, S. Agrawal, D. Becher, R. Bigwood, M. Buehler, V. Chikarmane, M. Childs, J. Choi, S. Daviess, C. Ganpule, J. He, P. Hentges, I. Jin, S. Klopcic, G. Malyavantham, B. McFadden, J. Neulinger, J. Neirynck, Y. Neirynck, C. Pelto, P. Plekhanov, Y. Shusterman, T. Van, M. Weiss, S. Williams, F. Xia, P. Yashar, A. Yeoh, Low-k interconnect stack with a novel self-aligned via patterning process for 32 nm high volume manufacturing, Conference Proceedings of the IEEE International Interconnect Technology (IITC) 2009, pp. 249–251.
[6] S.M. Smith, T. Tighe, D. Convey, J. Quintero, Y. Wei, Conversion of a plasma enhanced chemical vapor deposited silicon–carbon–nitride thin film at ultra-low temperature by oxygen plasma, Thin Solid Films 516 (2008) 885–890.
[7] I. Martin, M. Vetter, A. Orpella, C. Voz, J. Puigdollers, R. Alcubilla, Surface passivation of n-type crystalline Si by plasma-enhanced-chemical-vapor-deposited amorphous SiC_x:H and amorphous SiC_xN_y:H films, Appl. Phys. Lett. 81 (2002) 4461–4463.
[8] H. Cui, P.A. Burke, Time-dependent dielectric breakdown studies of PECVD H:SiCN and H:SiC thin films for copper metallization, J. Electrochem. Soc. 151 (11) (2004) G795–G800.
[9] N. Fainer, Y. Rumyantsev, M. Kosinova, E. Maximovski, V. Kesler, V. Kirienko, F. Kuznetsov, Low-k dielectrics on base of silicon carbon nitride films, Surf. Coat. Technol. 201 (2007) 9269–9274.
[10] E. Vassallo, A. Cremona, F. Ghezzi, F. Dellera, L. Laguardia, G. Ambrosone, U. Coscia, Structural and optical properties of amorphous hydrogenated silicon carbonitride films produced by PECVD, Appl. Surf. Sci. 252 (2006) 7993–8000.
[11] A. Mallikarjunan, A.D. Johnson, L. Matz, R.N. Vrtis, A. Derecskei-Kovacs, X. Jiang, M. Xiao, Silicon precursor development for advanced dielectric barriers for VLSI technology, Microelectron. Eng. 92 (2012) 83–85.
[12] M. Tada, H. Yamamoto, F. Ito, T. Takeuchi, N. Furutake, Y. Hayashi, Chemical structure effects of ring-type siloxane precursors on properties of plasma-polymerized porous SiOCH films, J. Electrochem. Soc. 154 (7) (2007) D354–D361.

[13] C.H. Lo, M.H. Lin, K.S. Liao, M.D. Guzman, H.A. Tsai, V. Rouessac, T.C. Wei, K.R. Lee, J.Y. Lai, Control of pore structure and characterization of plasma-polymerized SiOCH films deposited from octamethylcyclotetrasiloxane (OMCTS), J. Membr. Sci. 365 (2010) 418–425.
[14] H.E. Tu, Y.H. Chen, J. Leu, Low-k SiC_xN_y films prepared by plasma-enhanced chemical vapor deposition using 1,3,5-trimethyl-1,3,5-trivinylcyclotrisilazane precursor, J. Electrochem. Soc. 159 (5) (2012) G56–G61.
[15] S.M. Sze, Physics of Semiconductor Devices, John Wiley and Sons, Inc., New York, 1981.
[16] M.R. Baklanov, K.P. Mogilnikov, Non-destructive characterisation of porous low-k dielectric films, Microelectron. Eng. 64 (2002) 335–349.
[17] D.W. Gidley, W.E. Frieze, T.L. Dull, J. Sun, A.F. Yee, C.V. Nguyen, D.Y. Yoon, Determination of pore-size distribution in low-dielectric thin films, Appl. Phys. Lett. 76 (2000) 1282–1284.
[18] B. Lee, Y.H. Park, Y.T. Hwang, W. Oh, J. Yoon, M. Ree, Ultralow-k nanoporous organosilicate dielectric films imprinted with dendritic spheres, Nat. Mater. 4 (2005) 147–151.
[19] B. Lee, J. Yoon, W. Oh, Y. Hwang, K. Heo, K.S. Jin, J. Kim, K.W. Kim, M. Ree, In-situ grazing incidence small-angle x-ray scattering studies on nanopore evolution in low-k organosilicate dielectric thin films, Macromolecules 38 (2005) 3395–3405.
[20] A. Guinier, G. Fournet, Small-Angle Scattering of X-rays, John Wiley & Sons, New York, 1955.
[21] S. Nagarajan, M. Li, R.A. Pai, J.K. Bosworth, P. Busch, D.-M. Smilgies, C.K. Ober, T.P. Russell, J.J. Watkins, An efficient route to mesoporous silica films with perpendicular nanochannels, Adv. Mater. 20 (2008) 246–251.
[22] V. Jousseaume, O. Gourhant, A. Zenasni, M. Maret, J.-P. Simon, Grazing incidence small angle x-ray scattering study of the structure of nanoporous ultralow-k dielectrics prepared by plasma enhanced chemical vapor deposition, Appl. Phys. Lett. 95 (2009) 022901.
[23] R.J. Roe, Methods of X-ray and Neutron Scattering in Polymer Science, Oxford University Press, New York, 2000.
[24] A. Guinier, La diffraction des rayons X aux tres petits angles; application a l'etude de phenomenes ultramicroscopiques, Ann. Phys. 12 (1939) 161–237.
[25] D.J. Kinning, E.L. Thomas, Hard-sphere interactions between spherical domains in diblock copolymers, Macromolecules 17 (1984) 1712–1718.
[26] K. Heo, S.G. Park, J. Yoon, K.S. Jin, S. Jin, S.W. Rhee, M. Ree, Quantitative structure and property analysis of nanoporous low dielectric constant SiCOH thin films, J. Phys. Chem. C 111 (2007) 10848–10854.
[27] H. Shimizu, N. Tajima, T. Kada, S. Nagano, Y. Ohashi, S. Hasaka, Novel precursor for development of Si-C_2H_4-Si networks in SiCH for application as a low-k cap layer beyond 22 nm nodes, Jpn. J. Appl. Phys. 49 (2010) 05FF02.
[28] S.M. Gates, D.A. Neumayer, M.H. Sherwood, A. Grill, X. Wang, M. Sankarapandian, Preparation and structure of porous dielectrics by plasma enhanced chemical vapor deposition, J. Appl. Phys. 101 (2007) 094103.
[29] A. Grill, D.A. Neumayer, Structure of low dielectric constant to extreme low dielectric constant SiCOH films: fourier transform infrared spectroscopy characterization, J. Appl. Phys. 94 (2003) 6697–6707.
[30] A.M. Wrobel, I. Blaszczyk-Lezak, A. Walkiewicz-Pietrzykowska, T. Aoki, J. Kulpinski, Hard and high-temperature-resistant silicon carbonitride coatings based on N-silyl-substituted cyclodisilazane rings, J. Electrochem. Soc. 155 (4) (2008) K66–K76.
[31] Z. Chen, K. Prasad, C.Y. Li, S.S. Su, D. Gui, P.W. Lu, X. He, S. Balakumar, Characterization and performance of dielectric diffusion barriers for Cu metallization, Thin Solid Films 462–463 (2004) 223–226.
[32] Y. Taki, T. Kitagawa, Osamu Takai, Shielded arc ion plating and structural characterization of amorphous carbon nitride thin films, Thin Solid Films 304 (1997) 183–190.